Ecological Informatics 81 (2024) 102628

Contents lists available at ScienceDirect

Ecological Informatics

journal homepage: www.elsevier.com/locate/ecolinf

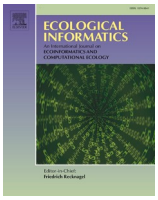

Revealing forest structural "fingerprints": An integration of LiDAR and deep learning uncovers topographical influences on Central Amazon forests

Nathan Borges Gonçalves [a,b,*], Diogo Martins Rosa [c], Dalton Freitas do Valle [c], Marielle N. Smith [d], Ricardo Dalagnol [e,f], Danilo Roberti Alves de Almeida [g], Bruce W. Nelson [c], Scott C. Stark [a,b]

[a] Michigan State University, Department of Forestry, College of Agriculture & Natural Resources, East Lansing, MI, USA
[b] Program in Ecology, Evolution, and Behavior, Michigan State University, East Lansing, MI, USA
[c] INPA – National Institute for Amazon Research, Manaus, AM, Brazil
[d] School of Environmental & Natural Sciences, College of Environmental Sciences and Engineering, Bangor University, Bangor, UK
[e] Center for Tropical Research, Institute of the Environment and Sustainability, University of California Los Angeles (UCLA), Los Angeles, CA 90095, USA
[f] NASA-Jet Propulsion Laboratory, California Institute of Technology, Pasadena, CA 91109, USA
[g] Department of Forest Sciences, "Luiz de Queiroz" College of Agriculture, University of Sao˜Paulo (USP/ESALQ), Piracicaba, SP, Brazil

ARTICLE INFO

Keywords:
Structural "fingerprints"
LiDAR
Deep learning
Amazon Forest
Terrain variation

ABSTRACT

Amazon forests are characterized by rich structural diversity. However, the influence of factors such as topography, soil attributes, and external disturbances on structural variability is not always well characterized, and traditional structural metrics may be inadequate to capture this type of complexity. While LiDAR offers expanded structural insights, traditional parameters used in LiDAR analysis, such as mean or maximum canopy height, are not always well directly linked to environmental variables like topography. Emerging approaches merge LiDAR with machine learning to uncover deeper structural complexities. However, work to date may fail to fully utilize the potential of fine-scale LiDAR information. Here we introduce a novel approach, leveraging 2D point cloud images derived from a profiling canopy LiDAR (PCL). The technique targets intricate details within LiDAR point clouds by using deep learning algorithms. With a dataset from the Central Amazon comprising 18 multitemporal transects of 450 m in length, our objective was to detect structural "fingerprints" of varied topographical types along a hillslope, comprising: Riparian, White-sand, and Plateau, and to detect any gradient of structural shifts based on terrain variations here represented by the height above the nearest drainage (HAND). The dataset was trained and tested using a leave-one-group-out approach (LOGO) in which, for each iteration, a complete 450 m multitemporal transect was excluded from training and tested after each iteration. The fast.ai platform and a ResNet-34 architecture, coupled with transfer learning, were used to perform a classification to distinguish between three topographical types. Furthermore, a hybrid model combining a Convolutional Autoencoder, and Partial Least Square (PLS) regression was designed to detect forest structural gradient correlations with HAND variation. Cross-validation achieved a promising high weighted F1 score of 0.83 to classify forests based on the topographical types. Additionally, a combined Convolutional Autoencoder and PLS regression revealed a strong correlation ($R^2 = 0.76$) between actual and predicted HAND. Innovatively combining deep learning with ground-based PCL LiDAR, our study revealed unique Amazon Forest structures connected to topographic variation. Our findings underscore the transformative potential of such integrative approaches for investigating forest dynamics and promise a powerful new tool for understanding climate-related forest structure change.

1. Introduction

Understanding and describing forest structural characteristics and the factors that influence them is crucial for determining the ecological processes underpinning forested ecosystems (Ehbrecht et al., 2021; Li et al., 2023). This knowledge is key to understanding the impact of climate change on forests, and to guiding future conservation and restoration efforts (; Rödig et al., 2018; Almeida et al., 2019; Atkins

* Corresponding author at: Michigan State University, Department of Forestry, College of Agriculture & Natural Resources, East Lansing, MI, USA.
E-mail address: nathanborges@gmail.com (N.B. Gonçalves).

https://doi.org/10.1016/j.ecoinf.2024.102628
Received 22 October 2023; Received in revised form 30 April 2024; Accepted 2 May 2024
Available online 5 May 2024

et al., 2020). Forests in the Amazon have structural arrangements that include variations in the stratification of the canopy, surface rugosity, frequency of gap sizes, spatial clustering of leaf age classes and leaf quantity that fluctuate seasonally (Lopes et al., 2016; Smith et al., 2019; Dalagnol et al., 2021; Gonçalves et al., 2023; Gorgens et al., 2023). Several factors may affect these arrangements at a local scale, including topography, soil drainage, soil texture, soil chemistry, local climate, human activity, and microburst-driven blowdowns (Quesada et al., 2012; Schietti et al., 2014; Araujo et al., 2017). A large body of evidence suggests that topography in the Central Amazon is closely related to changes in soil texture and water table depth, which influence tree species composition and several other plant life forms (Schietti et al., 2014; Dalagnol et al., 2022). Other factors may also play a role at the basin scale, in addition to those mentioned at the local scale. For example, it has been suggested that soil fertility and physical properties, climate, and anthropogenic disturbances may impact plant mortality and growth rates (Toledo et al., 2011, Quesada et al., 2012, Aleixo et al., 2019), and affect gap formation patterns (Dalagnol et al., 2021; Gorgens et al., 2023; Stark et al., 2012; Dalagnol et al., 2021; Gorgens et al., 2023; Simonetti et al., 2023). These responses may generate distinct forest structures, including biomass and maximum and mean heights in plots (Gorgens et al., 2021). Forests may have different “structural signatures” due to a combination of these factors. Consequently, the structure of a forest can provide clues about its disturbance history (Fahey et al., 2019; Atkins et al., 2020; Jucker, 2022, Smith et al., 2023), soil fertility, soil drainage, and species composition.

Traditional univariate methods and low-resolution metrics from forest inventories may not adequately capture the full range of structural complexity and variability observed in forest ecosystems (Hardiman et al., 2011; Atkins et al., 2020; LaRue et al., 2023). Particularly in the Amazon, where the intricate interplay of topography and soil attributes may define forest structures, univariate forest structure metrics may not be suitable. For instance, Suominen et al. (2015) found that, despite large differences in soil properties and tree species compositions across sites in the Peruvian Amazon, similar forest structures were observed using simple forest structure metrics, such as stem density and a gap fraction. A plot-based study in the Central Amazon found that only 20% of the variance in above-ground biomass (a common structural parameter) could be accounted for by topography and soil at the 1-ha sample scale ($n = 72$; Castilho et al., 2006). These findings point towards the importance of adopting more nuanced and comprehensive methods, like LiDAR, to accurately capture the complex interplay between forest structure and environmental factors. LiDAR provides fine-scale information and a broader suite of structural attributes (Reis et al., 2022), some of which may be more strongly related to environmental factors. Despite this, studies investigating the relationship between forest structure derived from airborne LiDAR surveys and topography in tropical forests have primarily relied on canopy height or gap fraction metrics as a proxy for forest structure (Detto et al., 2013; Jucker et al., 2018). These studies suggest that only a small portion of the variation in these structural variables is directly related to topographical factors.

Acknowledging the limitations of univariate approaches in examining the interplay between environment and forest structure, recent advancements in the use of LiDAR in forest ecology have sought to offer more in-depth and comprehensive insights. It has been shown that a multidimensional approach to describing forest structure is more likely to produce better results in describing forest complexity and its relation to function (Hardiman et al., 2011; Fahey et al., 2019; Murphy et al., 2022; LaRue et al., 2023). Notably, the integration of LiDAR and machine learning algorithms has emerged as a promising avenue for such evaluations. A pioneering study by Almeida et al. (2019) obtained several forest structural attributes from a ground-based profiling canopy LiDAR (PCL). These were combined with machine learning to classify forest types associated with different past land uses. Atkins et al., 2020 used a similar approach with ground-based lidar in North America and Scheeres et al. (2023) employed UAV-borne LiDAR data and a random forest classifier to separate forest types within restoration landscapes in southeastern Brazil. However, a possible limitation of these studies was the reliance on simple descriptive statistics to summarize complex point cloud data for a few, relatively large sample units. This tends to homogenize the 2D/3D point cloud and eliminate any spatial features contained in the data that could hide important forest structural complexities. Consequently, machine learning models may become more difficult to train, potentially compromising their robustness and generalizability.

To fully harness the capabilities of LiDAR-derived data, we advocate for adopting multidimensional analyses that leverage the entirety of the information in a 2D/3D point cloud. Considering the upward-looking transect-based LiDAR, the point cloud is two-dimensional, with time or distance on the x-axis and pulse return heights on the z-axis. These are 2D scatterplots that can be split into discrete portions of space along-track (with a predefined x-axis length), creating 2D images with sufficient samples for visual deep learning algorithms. Such algorithms can delve deeply into complex datasets, potentially revealing spatial patterns and correlations that are otherwise concealed via alternative methods. Drawing an analogy from animal ecology, this transformation resembles how sound data is converted into spectrograms: by segmenting sound into brief time intervals and subsequently calculating frequency spectra for each span (McGinn et al., 2023). These "sound images", when combined with deep learning algorithms, have demonstrated significant success in various classification tasks (Lee et al., 2009). A similar methodology applied to LiDAR data for forest science applications, could be equally transformative.

Here, our main objective is to test a novel approach to analyzing LiDAR data in the context of forest ecology. In this approach, LiDAR point clouds are transformed into images and deep learning techniques are applied. We use a ground-based profiling canopy LiDAR (PCL) multi-temporal dataset sourced from a small yet representative region in the central Amazon. The area is characterized by a marked gradient in soil texture and soil drainage along a mature hillslope or topographic profile, with LiDAR surveys conducted at high, medium, and low points along the topographic gradient that we refer to as Plateau (p), White-sand (w), and Riparian (r), respectively. These topographical gradients are ideal for exploring the relationships between terrain variation and forest structure, offering unique insights into the ecological dynamics of this region. We use this unique, multi-temporal LiDAR dataset to investigate our main objective and test two key hypotheses, posed as specific questions: (1) Can the structural characteristics captured in LiDAR-derived Forest structural images effectively differentiate between Plateau (p), White-sand (w), and Riparian (r) topographical types in the central Amazon? Essentially, do these topographical types exhibit distinct forest structural "fingerprints" in LiDAR-derived images? And (2) Is there a detectable gradient of structural changes (from LiDAR) within these forests that correlates with variations in terrain? In other words, can we identify forest structural shifts within these forests along the terrain gradient? We compare our image-based technique to a traditional approach that employs summary statistics to extract information from the 2D point clouds.

2. Methods

2.1. Study area

The study area covers about eight square kilometers near the field base of the Large-Scale Biosphere-Atmosphere Program in the Amazon (LBA) of the National Institute of Amazonian Research (INPA), about 60 km northwest of the city of Manaus, Brazil. The topographical gradient was derived from preferential dissolution and export of kaolin clay and by biological cycling of Si, under a stable humid tropical climate with minimal physical erosion (Chauvel et al., 1987). The loss of clay fraction accelerates where there is a horizontal component to soil water flow direction. This leads to differential chemical deflation of the landscape

being more advanced on lower slopes and valley bottoms.

To capture the topographic gradient, six 150 m transects were established in each topographical type, i.e., to top, bottom and middle sections of the topography (Fig. 1). LiDAR measurements of forest structure were made in each transect monthly between March 2015 and March 2016, always close to the 15th of the month.

2.2. Delimitation of environments and placement of transects

To delineate the three environments associated with sections of the local topography, we obtained HAND values (Height Above the Nearest Drainage) for all 30x30m raster cells. We start with a Digital Elevation Model of elevations above sea level. The HAND value of a cell is its vertical height above a reference surface interpolated between all stream thalweg cells having running water. Thalweg cells are those whose contributing area of runoff from upslope cells exceeds a locally verified threshold of 24 ha (270 raster cells) (Rennó et al., 2008; Nobre et al., 2011; Schietti et al., 2014). The starting DEM was from the year 2000 based on the Shuttle Radar Topography Mission (Fig. 1C). Pre-processing steps for obtaining the "upslope contributing area" raster included (a) 3 × 3 cell moving average to smooth out irregularities in the DEM caused by forest canopy rugosity, (b) pit-filling, and (c) flow-direction raster. We obtained the slope value of each DEM cell from the smoothed DEM.

The locations of six transects for each of the three topographical segments were identified using HAND intervals of >40 m for clay soil Plateau forest, 8–20 m for forests on White-sand, and < 1 m for water-logged Riparian forest on White-sand. Slopes were confined to <6 degrees to minimize topographic shading in a Landsat image. Furthermore, mature White-sand podzol does not develop on steep slopes, probably due to mechanical erosion (Chauvel et al., 1987). Samples were spread over ~8 km^2 within the footprint of a micromet tower (K34). Soil samples were collected to characterize the soil texture gradient as percentages of clay, silt and sand. Fourteen composite samples were obtained per environment, at a depth of 25 cm below the organic matter horizon. Analyses followed the EMBRAPA (1997) pipette method. The transects were allocated using a GARMIN MAP 62S GPS and a compass, maintaining a single azimuth for each transect.

2.3. Portable terrestrial LiDAR system

The portable range-finder LiDAR is model LD90-3100VHS-FLP, manufactured by Riegl (Horn, Austria). Each pulse is contained in an oval-shaped beam footprint with a 6x4cm major and minor axes near the sensor and 15x3 cm at 45 m distance. The instrument provides 1000 last-return distances from 1000 pulses per second. Pulses that do not return are presumed not to hit an object. These are called skyshots and are encoded as zero distance. The emitting and sensing lenses are in the same instrument, held with a vertical upward view while traversing a transect at constant walking speed. This provides a two-dimensional cloud of last returns (x, z), with x being the along-track distance and z being the last-return height above the ground. The sensor's wavelength is 900 nm (near-infrared), which is strongly reflected by leafy vegetation. The accuracy is ±25 mm, and the nominal range is 200 m without a reflector. The instrument provides alternating first and last returns, but only the last returns were used to avoid overestimating understory density, and to follow the protocol of previous studies (Parker et al., 2004; Parker and Russ, 2004; Stark et al., 2012).

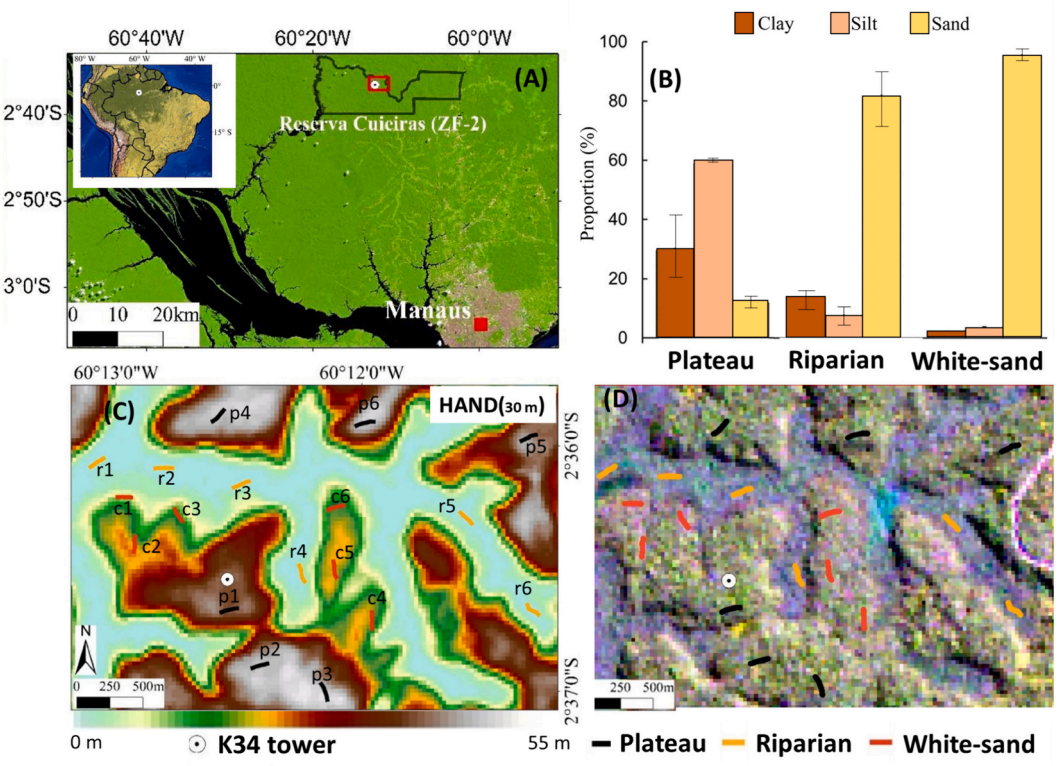

Fig. 1. **A**) Location of the study site (K34); **B**) Clay, sand and silt proportion in the three topographical segments: upland Plateau on well drained ferralsol, White-sand, characterized by podzolic soils on the gradual inclines of lower slopes, and Riparian forest on sandy soil with permanently high water table; **C**) Placement of transects in the three topographical sections (18 transects in total, each 150 m in length, six per topographical segment), where the topographical gradient is represented by vertical Height Above Nearest Drainage (HAND); **D**) Landsat 8 false-color RGB image using short-wave infrared, near infrared, and red bands. This figure was modified from Rosa et al., 2017. Plateaus and steep upper slopes are well-drained clay-rich Ferralsol (FAO)s; gradual lower slopes are on White-sand tropical Podzols with a surface root mat; riparian zones have permanently waterlogged sandy soils with thick leaf litter accumulation (Chauvel et al., 1987; Luizão et al., 2004). (For interpretation of the references to color in this figure legend, the reader is referred to the web version of this article.)

The LiDAR is attached to a short pole and held one meter above the ground. Two operators are required. The first is responsible for walking at a constant speed along the transect, and the second is responsible for starting and stopping the recording and saving the data on a PC computer. A rope marked every two meters and a metronome installed on the PC helped maintain a constant speed. In this way, we obtained ~2300 last returns per linear meter of transect, or a two-dimensional cloud containing the positions of reflective vegetation (x, z) for ~345,000 last returns in each 150 m transect.

2.4. Generation of 2D point clouds using PCL LiDAR

To transform PCL LiDAR raw data into 2D point cloud images, we first segmented each 150 m transect into 5-m sections, producing 30 images per transect totaling (18*30 = 540). Plots below show examples of 5 m along-track slices of last return heights using the ggplot2 (Wickham, 2016) density function (*geom_bin2d(bins = 90))* in R (R core team, 2020). Each panel is a two-dimensional histogram (Fig. 2) where the color of each square bin represents the point counts within a particular area of the plot. 2D point cloud images were confined to vertical distances ranging from 2 m to 36 m. This range was selected to mitigate the impact of structural interference from LiDAR walk below 2 m and also to eliminate outliers above 36 m. These measures were also taken to facilitate the deep learning model's performance and to fit the data more effectively into a square image format (Fig. 2). The resulting images can then be used for further analysis.

To expand our dataset, we tripled the image pool for each transect by incorporating multi-temporal data. By drawing data from a three-month span (March, September and October 2015) across three environments, we could more effectively train and test deep learning models, which inherently demand many images to learn effectively, however, increasing the number of time periods by more than three was not possible, given a limitation in our processing resources (we used Google Colab, https://colab.research.google.com, and GPU was limited). These particular months were selected at random from those with the highest seasonal Leaf Area Index (LAI), as identified by Wu et al. (2016). Utilizing this multi-temporal data, a single 150 m transect from any given environment effectively yielded 450 m of transect data (hereafter multitemporal transect). This is because each 150 m transect was surveyed over the three separate time periods, thereby tripling the length of data for analysis. Consequently, the total number of images available for the training process to answer **Q1** and **Q2** amounted to 1620, which is 450 m divided by 5 m intervals, multiplied by 18 (the number of transects) = 1620 images (Fig. 3).

2.5. Framework for analyzing Forest structure complexity using LiDAR-derived 2D point cloud images using deep learning

To address our two questions, we adopted a two-fold methodology, involving the same set of the 1620 2D point cloud images derived from 18 multitemporal transects and the Leave-One-Group-Out (LOGO) cross-validation. We believe the two main questions posed here can be answered by using deep learning algorithms: a classification task for **Q1** and a regression task for **Q2**. In our framework, each 5 m wide image segment, derived from each 450 m multitemporal transect, is the primary unit for model training. However, to derive final predictions for each multitemporal transect, we employ a majority voting strategy on the predictions made for individual 5 m image segments, aligning with our overarching objective of accurately predicting the entire multitemporal transect. For the classification task, every image is assigned a topographic type label – either "Plateau", "White-sand", and "Riparian", corresponding to the respective topographical type. In the regression

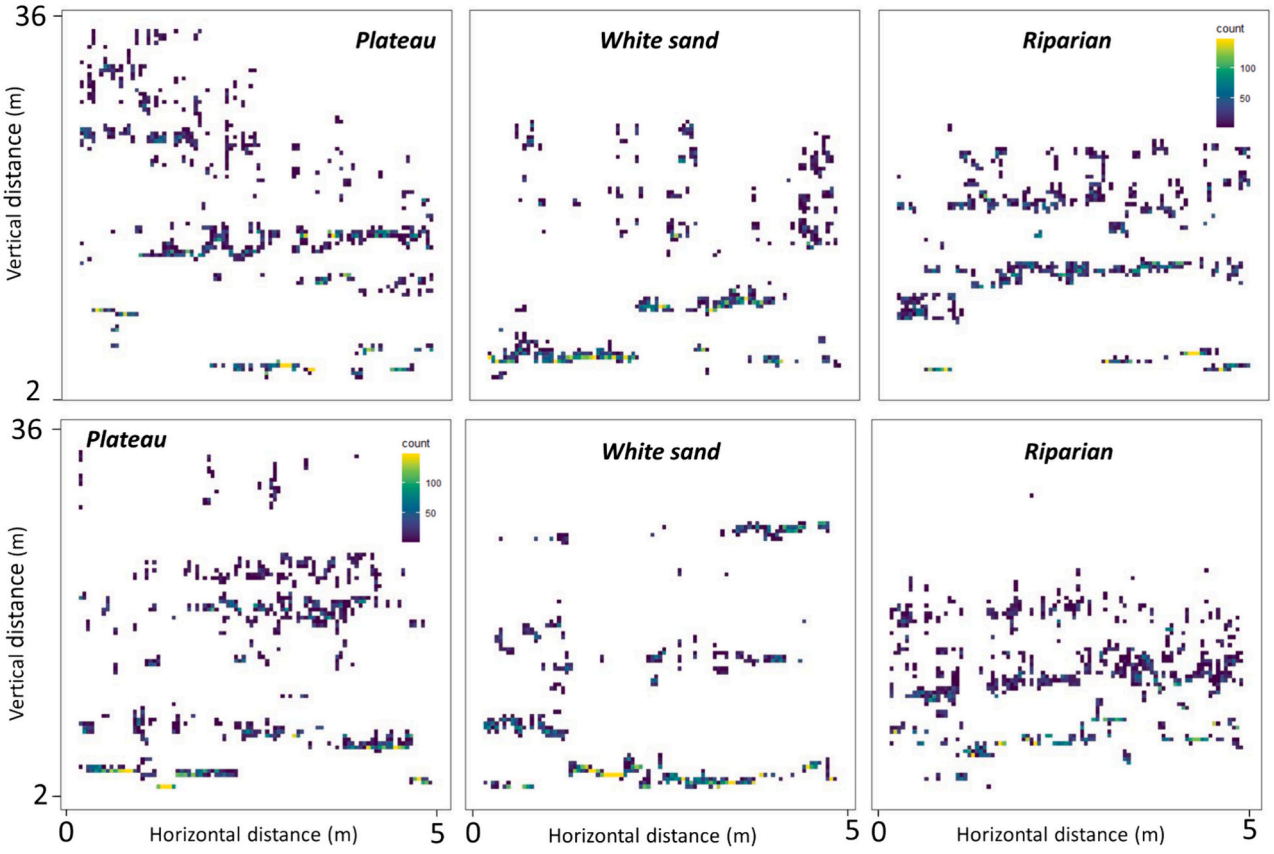

Fig. 2. Examples of 5 m squared binned frequencies from 2D point clouds, used to train the classifier and the regression algorithms (**Q1** and **Q2**). In general, Riparian forests had a more compact point cloud, White-sand forests had more gaps and Plateau Forest was taller and had more layers (*personal observation*).

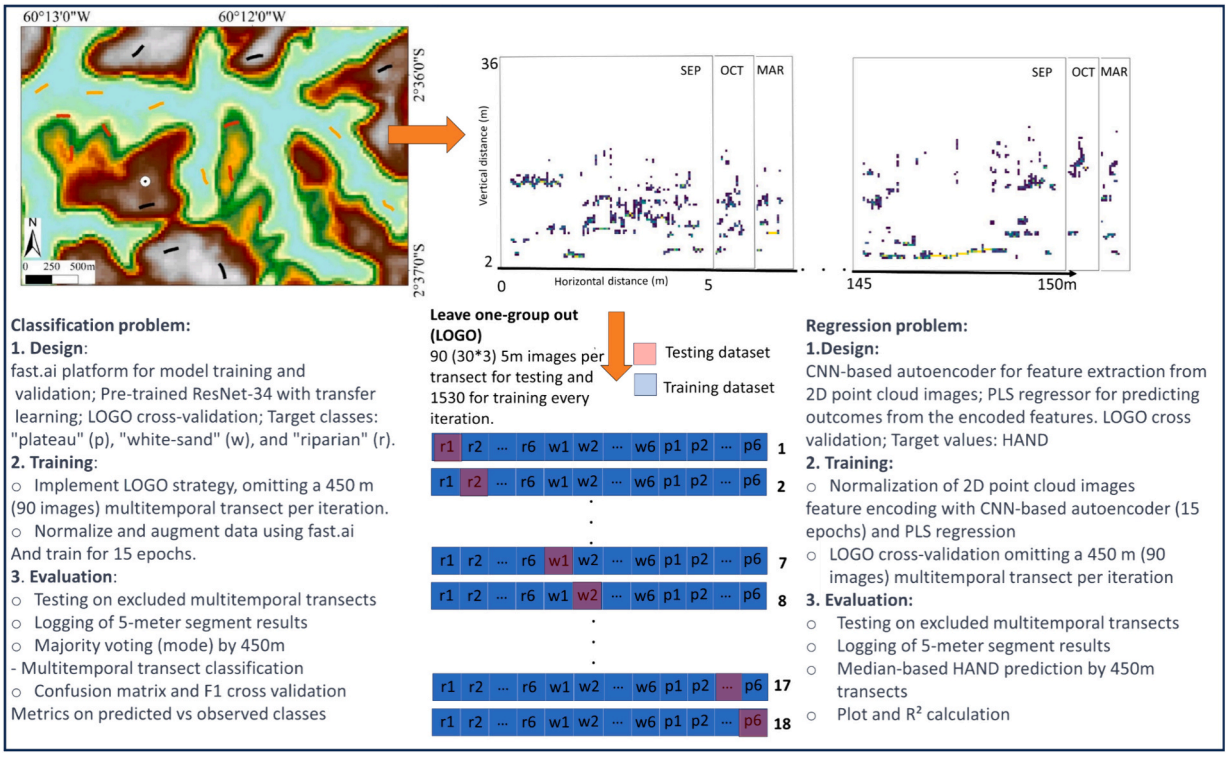

Fig. 3. Schematic illustration detailing the LiDAR data segmentation into 5-m image slices for each multitemporal transect. The diagram also summarizes the training methodology employed for both regression and classification problems, emphasizing the leave-one-group-out (LOGO) cross-validation approach and the majority voting strategy.

task, each image segment is associated with a continuous value of Height Above the Nearest Drainage (HAND) at the respective multitemporal transect. These labels and values represent our targets for the training and testing process. As a result, in our LOGO approach one entire multitemporal transect with 90 images is left out and the 1530 images of the remaining 17 multitemporal transects are used to train the data. The model is retrained for each fold, ensuring that there is no information transfer or contamination from previous folds. Considering the nature of our multitemporal dataset, where the same transect (150 m) measured over time is not independent, we had to exclude a complete 450 m multitemporal transect, comprising 90 images, from each iteration for testing purposes. Our initial focus was on a classification task aimed at addressing our first question: Can we distinguish between three distinct topographical types in terms of forest structure using ground-based LiDAR-derived 2D point cloud images? Following this, in order to depict the gradual variations in forest structure along the terrain, we employed a regression approach to answer **Q2**. This involved using the same 2D point cloud images representing forest structures to predict their corresponding topographical variation represented by the HAND (Height above the nearest drainage). A diagram illustrating the workflows of the two approaches that tackle both questions is shown in Fig. 3.

2.5.1. Classification problem (Q1): Deep learning applied to 2D LiDAR images for Forest classification

We employed the fast.ai platform (Howard and Gugger, 2020) to train and validate models for the classification of 2D point cloud images, utilizing a LOGO (Leave-One-Group-Out) cross-validation. In this approach, our target classes were "Plateau", "White-sand", and "Riparian", designated as "p", "w", and "r" respectively. In each iteration, a complete 450 m multitemporal transect was omitted from the training process (the grouping factor giving the lack of independence in the multi-temporal data) and subsequently tested. This approach ensured an assessment of the model's performance, accounting for our data constraints and guaranteeing that every multitemporal transect undergoes both training and testing. A critical point to highlight is that models are retrained for each fold, preventing previous fold's information from being transferred. We utilized the pretrained ResNet-34 (Which consists of a 34-layer convolutional neural network) architecture which is a variant of the ResNet (Residual Network) family, widely used for deep learning tasks, particularly in computer vision (He et al., 2016). ResNet-34 was used inside the fast.ai framework (Howard and Gugger, 2020) to leverage existing knowledge, this is particularly useful in our dataset since its small size. Transfer learning generally consists in using a model pre-trained on broad datasets, like ImageNet (Deng et al., 2009), to specialized tasks with more limited data. As part of the cross-validation of the Leave-One-Group-Out approach, the test directory containing the multitemporal transect was temporarily moved to test, and *DataLoaders* were created using the remaining image files from the other 17 multitemporal transects. We applied automatic data augmentation in fast.ai and normalization using the ImageNet statistics, this process includes resizing the images to 224 × 224 pixels. We utilized a learning rate of 0.007 and 15% of the training data was used for training validation purposes. We trained the models for 15 epochs for each iteration. After each training iteration, we restored the test directory and predicted the topographical type for the left-out multitemporal 450 m (90 images) transect using the trained model on the other 17 multitemporal transects. The predictions were then saved in a text file for further analysis.

Using a Leave-One-Group-Out, each multitemporal 450 m transect's final classification was based on the dominant prediction class (or simply the Mode) from the 90 individual 5 m wide images within it. Leveraging the majority classification of these segments to identify a transect reduced the potential negative effects of misclassifying individual 5 m images. This approach is particularly crucial since variations like gap formations from tree deaths are common and expected, meaning that smaller segments might mimic the structural attributes of other classes. Additionally, our limited size in data training might not sufficiently capture finer structural nuances.

We evaluated the model's performance by calculating the broadly

used weighted F1 score. The F1 score is a harmonic mean of precision and recall, providing a balanced measure of both the false positives and false negatives in the classification results. To calculate the F1 score, we first obtained the true labels and predicted majority classes for each transect from the aggregated data. We then used the Python Scikit-learn (Pedregosa et al., 2011) library to compute the confusion matrix for the true and predicted labels, considering the three classes: "p", "w", and "r". Finally, we calculated the weighted F1 score using the f1_score function from Scikit-learn, specifying the true labels, predicted labels, and the average parameter set as "weighted".

We have also adopted a broader and more conservative cross-validation strategy to add robustness to the results we present here, as we only use ~5% of the data for every iteration in the previous method. This strategy involves excluding three multitemporal transects (~17% of the data) for testing in each iteration, specifically one from each target class - "Plateau" (p), "White-sand" (w), and "Riparian" (r). This is done to avoid strong imbalances in the training data. As we train less data in each iteration, we expect some decrease in model performance when compared to the previous approach. We use the same training parameters from before, also ensuring that each fold was not contaminated from previous folds as before. In total, this cross-validation approach involves 216 unique iterations, each excluding a different combination of one multitemporal transect from each class. Through these 216 iterations, the model will classify the three held-out multitemporal transects, leading to predictions of 648 multitemporal transects (36 predictions for each multitemporal transect). In order to measure the model's performance across all classified transects, a cumulative evaluation was performed. Instead of analyzing each iteration separately, we assess the model's effectiveness using the weighted F1 score, and a confusion matrix based on all 648 multitemporal transects predictions.

2.5.2. Regression problem (Q2): Unveiling the gradient of Forest structural shifts along a topographic gradient- a hybrid machine learning approach with convolutional autoencoders and partial least squares regression

To answer our second question: Could we discern a gradient of forest structural shifts in these forests based on terrain variations? To do that with our data, we developed a hybrid machine learning approach and simply represented terrain variation as the Height Above Nearest Drainage (HAND) at each multitemporal transect (18 in total). The fast.ai platform, although powerful, does not readily support image regression problems, which led us to devise an alternative approach. Our strategy aimed to predict the continuous value of HAND of each multitemporal transect using the same pool of 2D point cloud image data from the (**Q1**) classification problem as the primary input. To do that, we built a model that merged the capabilities of a Convolutional Autoencoder with a Partial Least Square regression (PLSR). This combination enabled us to draw upon the advantages of both deep learning and PLSR in addressing regression problems.

The Convolutional Autoencoder and its variations extracts the most critical features and minimizes noise within the training data (Kingma and Welling, 2019, Zhao et al., 2019, Bank et al., 2023). This process results in a compact and informative feature matrix, which is subsequently fed into the PLSR or any regression model. PLSR is particularly suitable for datasets that have undergone Convolutional Autoencoder processing, where the output is a flattened vector representing each image, and each vector element is a variable in a tabular form. PLSR excels in these scenarios with numerous correlated variables (Carrascal et al., 2009). In our case the final matrix is transformed into a vector that represents each image with a vector with over 8000 values, each one representing one variable as a tabular form. The image dataset is organized into 18 folders, one for each of the 450 m transects (150 m *3). The 5 m wide images are resampled to 128 × 128 pixels and then normalized by dividing by 255. Each folder contains images associated with a unique value of HAND represented as a continuous value. As we had only a single HAND value for each transect, this value was repeated for all the images within a multitemporal transect. We also adopted a leave-one-group-out (LOGO) cross-validation approach, where each multitemporal transect was used once as a test set while the remaining transects were used for training. The models are retrained for each fold, ensuring that there is no information transfer or contamination from previous folds. We trained the autoencoder with 15 epochs and used 15 components in the PLSR to make predictions every iteration.

In summary, in the first stage of the model, the Convolutional Autoencoder, is trained on the training 2D point cloud image data. The autoencoder, composed of an encoder and a decoder, learns to reconstruct the input image (Kingma and Welling, 2019). After training, the encoder part of the autoencoder is used to transform both the training and testing images into a lower-dimensional representation. The second stage of the model involves training a PLSR on the encoded training images (transformed into a vector) and their corresponding value of HAND. Once the model has been trained, it is deployed to predict the HAND of the test multitemporal transects. Similar to the classification problem where a majority voting strategy was utilized in the testing data, the median was computed for each 450 m multitemporal transect containing 90 2D point cloud images. Subsequently, these median values were plotted against the true HAND values to provide a visual comparison of the model's performance and show possible gradient of structural changes with HAND, coefficient of determination (R2) was also calculated. All code and data used in the analysis are on GitHub (https://github.com/Nathanborg/Decoding-Amazon-Forest-Structures-fingerprints-/). Moreover, an ANOVA was performed with the mgcv (Wood, 2011) package in R on the predicted median values from the regression model for the test data, (gam(Predicted_HAND ~ Topographical type), where "r" stands for Riparian, "w" for white sand, and "p" for plateau. We also tested models including the spatial structure to avoid any possible spatial autocorrelation effects in the parametric tests. This analysis aims to reveal whether significant differences in forest structure exist among these previous classified topographical types and to detect any significant forest structural gradients of change as predicted by 2D point cloud data. Plots related to this specific model were made using the mgcViz package (Fasiolo et al., 2020).

We have also adopted a broader and more conservative testing strategy as in the classification problem (**Q1**) involving excluding three transects (~17% of the data) for testing in each iteration, specifically one from each target class - "Plateau" (p), "White-sand" (w), and "Riparian" (r), cross-validation is the same as before with the classification problem (see **2.5.1)**. In order to measure the model's performance across all transects, a cumulative evaluation was also performed. Instead of analyzing each iteration separately, we assess the model using coefficient of determination (R^2) between true vs predicted for all 648 multitemporal transects predictions.

2.5.3. A comparative evaluation of traditional LiDAR-derived metrics and 2D point cloud image-based machine learning in Forest type classification and regression analysis

To provide a comparison between our 2D point cloud image-based methodology against "traditional" metrics for both the regression and classification problems (**Q2** and **Q1,** respectively), we calculated 11 common LiDAR-derived Forest structure metrics at the 5 m segment level within each multitemporal transect. As in our primary analysis, which analyzed 5 m segmented images from a 3-month period, our comparative analysis utilizes the same dataset, but instead of being transformed into 2D point cloud images, it utilizes 11 summary statistics that are commonly used in ground-based lidar studies to summarize 2D-point cloud data (Stark et al., 2012, Almeida et al., 2019, Smith et al., 2023). The metrics were calculated using the same heights used in the image analysis (from 2 m to 36 m). As before, a total of 1620 (30 segments*18 transects* 3 months) segments are used, and in this case the 5 m point cloud is summarized in 11 variables. For each 5 m segment we calculated, Maximum Height: defined as the maximum height of the last return-pulse within each 5-m segment along the transect; Canopy Rugosity: calculated by retrieving the 150 highest returns within every

5 m segment along the transect and computing their standard deviation (Parker and Russ, 2004). Average height: the average of the 150 highest heights within each 5 m segment. Skyshots_1m, Skyshots_5m and Skyshots_10m: the percentage of each 5-m segment without vegetation above 1.5 and 10 m canopy height, respectively; Leaf Area Density (LAD) average: computed as the average of the leaf area density profile for each 5-m segment. LAD_SD: calculated as the standard deviation of the leaf area density profile for each 5-m segment; Leaf Area Height Volume (LAHV): introduced in Almeida et al., 2019, it is the sum of the products of height and mean LAD at that height, for all 5-m segments of transect. Leaf Area Index (LAI): for each 5-m segment, computed as the sum of the LAD profile; and 99% Percentile Height: determined by finding the height of the 99% percentile of pulses for each segment. These variables were organized in a tabular format with 1620 rows and 11 columns variables for further analysis.

As with the 2D point cloud images we also used a Leave-one-group out (LOGO) approach as cross validation with one multitemporal transect (450 m) left out for testing and the remaining for training. We now use a Random Forest classifier for the classification problem for **Q1** and a Random Forest regressor and a PLSR for **Q2** to train and test the models for each iteration. Random Forest is considered one of the most popular and effective ensemble methods for classifying and regressing tabular data where multidimensionality exists and rigorous feature selection is not always needed (Cutler et al., 2007; Belgiu and Drăguţ, 2016; Ziegler and König, 2014). And it is broadly used in several ecology and remote sensing applications. In the same way as before (**2.5.1** and **2.5.2**), predictions are made for the test data after every iteration and saved for later analysis. We used the Random Forest using the RandomForest package in R (Liaw and Wiener, 2002). We tuned the mtry hyperparameter with the caret package in R (Kuhn, 2008) while keeping other hyperparameters at their default values. However, we explored variations in the ntree parameter, experimenting with settings of 500, 1000, 5000, and 10,000. With a cutoff of 0.7, we also tested models in which features are selected prior to training using the findCorrelation function in the Caret package in R. We also used a majority voting strategy, using the mode for classification **Q1** and the median for **Q2** regression (see **2.5.1** and **2.5.2**). In this process, each 5-m segment within a 450 m multitemporal transect is assigned a predicted class or a continuous value for regression. This side-by-side analysis allowed us to assess the relative performance, effectiveness, and accuracy of our novel image-based machine-learning approach in contrast to 'traditional' metrics-based methods.

3. Results

For the classification problem (**Q1**), we employed the Leave-One-Group-Out (LOGO) cross-validation and a majority voting strategy. In this approach, each of the 18 multitemporal transects, comprising 90 images each, was classified based on the mode prediction across all its 5-m segments. As depicted in Fig. 3, this method, where the multitemporal transect itself was the unit of classification (Using the majority voting strategy for all 5-m segments within a 450 multitemporal transect) in each iteration, achieved a weighted F1 score of 0.83 (Fig. 4**)**. In Fig. S6, we present the curves for loss and accuracy across epochs for each fold using the initial Leave-One-Group-Out (LOGO) training method, alongside the average accuracy and loss for all folds. We also used a variation of LOGO for **Q1** in a more conservative way using 3 multitemporal transects (~17% of the data) as testing for every iteration, which also showed a very high weighted F1 score of 0.76 (**Fig. S3**). The 'traditional' metrics-based approach, employing 11 commonly used forest structure metrics to summarize the 2D point cloud using the same number of sample units as the image analysis (1620) and the majority of voting strategy, produced a low weighted F1 score (0.33–0.48) in the three tested random forest ntree parameters (**Fig. S5**, for 500 ntree and prior tuned mtry = 3). Prior feature selection did not affect these results.

The regression problem (**Q2**), a combination of a Convolutional Autoencoder and a PLS regressor, also demonstrated strong predictive power in predicting HAND. As indicated by the coefficient of determination (R^2) value of 0.76 (**Fig. 5,** $p < 0.001$), there was a strong and significant relationship between the observed and predicted HAND of the multitemporal transects, indicating that forest structure shifts along the topographic gradient from low (r) to intermediate (w) and uphill (p). The observed HAND values ranged from 0 to 50 m, while the predicted ranged from 12 to 30 m (Giving these are medians from within multitemporal transect 5 m segments). A straightforward ANOVA conducted on the median values predicted by the regression model revealed a significant influence of topographical type on the dependent variable ($F(2) = 21.81$, $p < 0.001$). This result verifies the existence of a distinct gradient, as demonstrated by Fig. S2, which displays a 95% confidence interval for the aggregated median transects across the topographical types "w", "p", and "r". Such findings underscore the regression model's capacity to effectively differentiate among the three distinct topographical types (or forest types) through the use of 2D point cloud images depicting forest structure. A more conservative variation of our LOGO cross-validation method, utilizing three multitemporal transects (approximately 17% of the dataset) as the testing set for every iteration, also demonstrated a very high coefficient of determination ($R^2 = 0.79$, $p < 0.001$). An ANOVA was also conducted as before on the median values predicted by the regression models and revealed a significant influence of topographical type on the dependent variable ($F(2) = 44.28$, $p < 0.001$, **Fig. S4**). The baseline comparison for the regression problem using the conventional metrics-based approach, employing 11 common forest structure metrics presented a lower correlation compared to the image-based analysis ($p = 0.01$, $R^2 = 0.43$), for the PLS regression the correlation was not significant ($p = 0.29$).

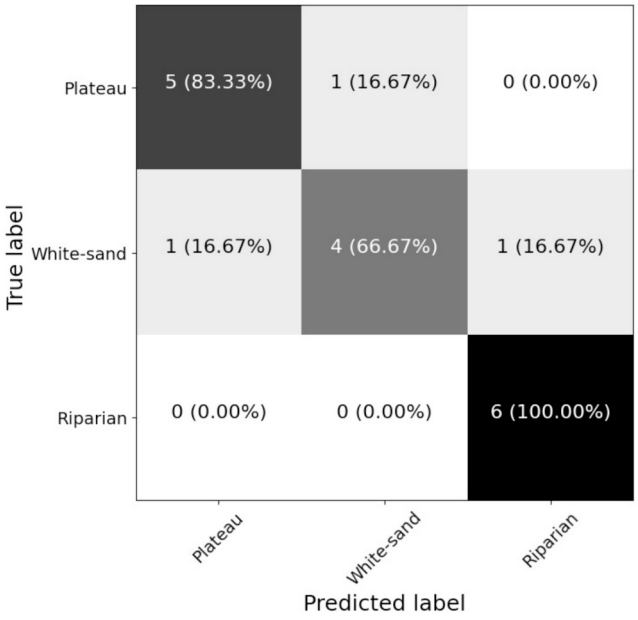

Fig. 4. Model performance confusion matrix when the validation set (1 entire multitemporal transect) is left out of the training process. True classes are in rows and predicted classes are in columns. Correctly classified segments fall along the diagonal from the top-left to the bottom-right. Shows classification accuracy of 83% when the majority voting strategy is applied, and the objects being classified are the eighteen multitemporal (3*150 m) 450 m transects. For each multitemporal transect of 450 m, the topographical class predicted most frequently (or simply the mode) among all of its 5-m segments is considered the final prediction for that multitemporal transect. Weighted F1 Score was 0.83.

4. Discussion

In this study, we explored a novel application of ground-based

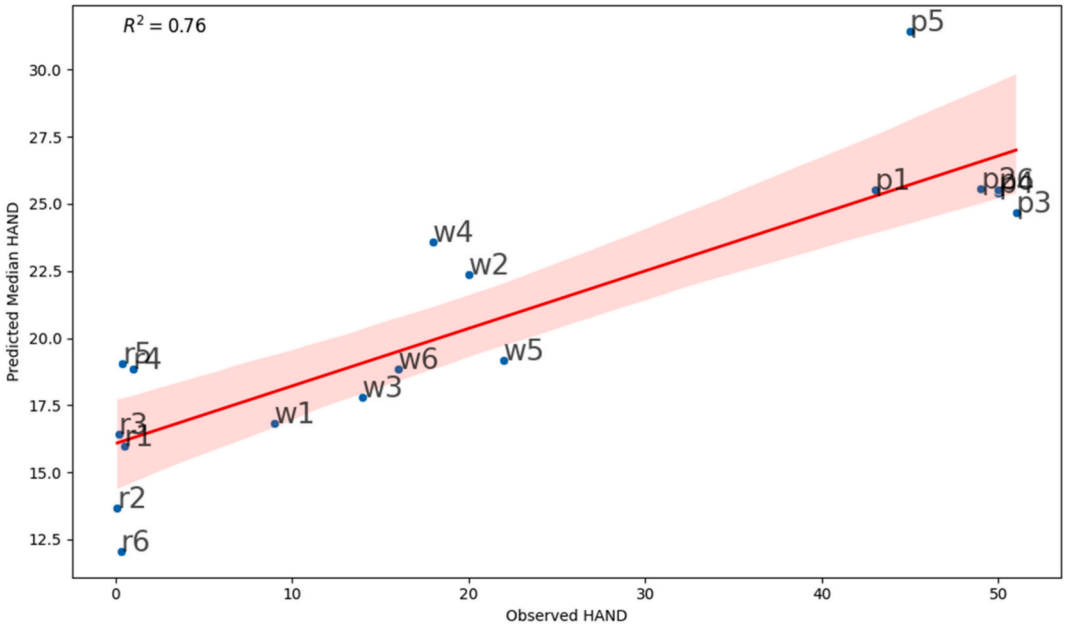

Fig. 5. A scatter plot showing our regression model's capability to estimate topographical variation, specifically the Height Above Nearest Drainage (HAND), based on density images depicting forest structures. Observed HAND values are shown on the x-axis, while median predicted HAND values are shown on the y-axis. Each data point on the graph corresponds to a distinct multitemporal transect. For a comprehensive evaluation, the median of all predicted HAND values within a given multitemporal transect (5mr segments) was computed to yield the final prediction. Symbol definitions: "r"–Riparian, "w"–White-sand, "p"–Plateau. Shaded red area in 95% of confidence interval.

canopy profiling LiDAR (PCL) data transformed into 2D point cloud images, combined with deep learning techniques, to discern forest structure "fingerprints" within the central Amazon, an area characterized by contrasting environmental gradients, particularly in soil and topography. Our approach set out to answer two primary questions: whether unique vertical forest "signatures" or "fingerprints" linked to different topographical types can be identified using LiDAR derived 2D point cloud images, and if there is a gradient of forest structural changes linked to the terrain gradient (Here represented by HAND). Our results affirmatively answer both these questions. This was reflected in the high accuracy our model achieved in classifying the testing multitemporal transects using 2D point cloud image data (weighted F1 score of 0.83), illustrating the effectiveness of our approach in identifying these unique forest structural patterns, and the strong correlation between predicted and observed Height above nearest drainage (HAND) ($R^2 = 0.76$) underscores the success in detecting these forest structure gradients along the hillslope.

Our approach is influenced by earlier research, including works by Almeida et al. (2019), Atkins et al. (2020), and Scheeres et al. (2023). These studies laid the groundwork by employing a "multidimensional" framework to analyze forest structure and classify forest types using LiDAR data. However, their main emphasis was on utilizing simple metrics, particularly in areas that are disturbed or undergoing regeneration. Here, we extend their foundational work by integrating deep learning techniques, which enabled a more in-depth exploration of the available data within an undisturbed old-growth forest. Our deep learning framework, even when trained with a limited dataset of just six transects per topographical type, effectively discerns fine-scale forest structures using 2D point cloud image data. This approach marks also a departure from previous studies like Almeida et al. (2019), Atkins et al. (2020), and Scheeres et al. (2023), which relied on summary statistics from larger sample units, essentially condensing entire 2D/3D point clouds into a few comprehensive metrics. In contrast, our method capitalizes on breaking down these larger units into more detailed 5-m segments of 2D point cloud image data.

To enable a comprehensive comparison with our proposed methodology, we also computed 11 prevalent structural metrics derived from LiDAR, utilizing identical multitemporal datasets employed in the image analysis for **Q1** and **Q2**. However, we segmented the data into 5 m segments, diverging from the previous approaches that aggregated data by plot (Almeida et al., 2019). This adjustment yields a dataset of 1620 continuous values for model training (90 values for each of the 450 multitemporal transects), as opposed to the limited dataset of 54 values that would result from summarizing the multitemporal transects. This approach resulted in suboptimal performance for both classification and regression tasks on the multitemporal transects when compared to the method proposed here (F1 score of 0.48 for classification and as high as R^2 of 0.43 for regression), strongly suggesting that important information may be lost when using summary statistics of 2D/3D point-cloud data. For the classification problem for example we would not be able to separate "r" Riparian from "w" White-sand forests based solely on these metrics (**Fig. S5**).

Utilizing image data, particularly in the form of density maps, presents significant advantages, especially when dealing with extensive datasets in the case of LiDAR point cloud returns, in our case each multitemporal transect sized about 24 MB (8*3) in raw return data while the images are compressed into 1 MB by multitemporal transect. In comparison to large tabular data with millions of rows, image data offers a more efficient and expedient processing alternative. For example, in the regression problem we used comparatively small 64 × 64 pixel images, thereby enabling faster computations. This approach is particularly beneficial when handling large datasets, as it requires fewer computational resources and less processing time than traditional methods. A similar approach, on a different application, was studied by Klauberg et al. (2023), where terrestrial LiDAR scanning (TLS) 3-D point cloud data of trees were simplified to 2-D images and used with a deep learning approach to classify tree damage from a hurricane. Furthermore, the ability of image data to encapsulate spatial relationships can offer additional insights that might be missed by other data forms, thereby enriching understanding of the structure of forests.

Despite the effectiveness of our majority voting strategy in identifying the most dominant class within each multitemporal transect, the models performance were lower when classifying individual 5 m segments (**Fig. S1**). This difference indicates that while our models can

accurately classify forest structure at larger scales, it is not as proficient at recognizing subtleties at smaller scales. However, this is an expected outcome given the inherent variability of natural forest structures. Factors such as tree mortality create gaps, leading to different stages of forest development within the same multitemporal transect. For example, one section of the transect may be in a regeneration phase while another is in a more advanced succession stage. Other than that, transects are more prone to have more variability than squared samples. This is because transects can span different environmental conditions or habitats within the same area. Future research should aim to enhance the classification of individual segments. This could be achieved by integrating additional data sources, such as 3DTerrestrial Laser Scan (TLS) data. By doing so, one could capture more of the nuanced variation within forests, leading to a more comprehensive understanding of these intricate ecosystems.

Our study underscores the link between topography and forest structure in the central Amazon. Our results indicate that varying terrains can give rise to distinct forest "signatures". Such unique patterns may hint at diverse species compositions and ecological processes, including varying water usage strategies. Several individual forest structure attributes could be behind these signatures; earlier analyses of the same dataset analyzed here indicated that Riparian and White-sand topographical types typically exhibit on average a shorter and more uniform canopy surface, as reported in Rosa et al., 2017 and partially shown in Fig. 2. Conversely, Plateaus situated on well-drained clay are characterized by a taller and more uneven canopy. These insights are crucial for understanding how forests, especially those with shallow water tables, adapt to drought conditions (Sousa et al., 2022, Costa et al., 2023). The variations in structure suggest that certain topographical-related adaptations might help these forests tolerate moderate water stress. However, the risk posed by intense droughts highlights the need for a deeper exploration into the relationship between topography, forest structure, and water availability (Esteban et al., 2021; Costa et al., 2023).

5. Conclusions

In conclusion, our study successfully demonstrated the power and potential of combining ground-based LiDAR with deep learning algorithms to discern and characterize unique structural "fingerprints" as well as forest structure gradients within the central Amazon Forest landscape. This approach, employing image data instead of conventional tabular data, successfully detected distinct forest types arising from varying topography within a representative region in the central Amazon. Despite dealing with a limited dataset, our framework proved robust, achieving a high weighted F1 score in classifying transects with a strong relationship between predicted and observed HAND showing a gradient of forest structural changes. The application of this novel approach to different ecosystems and geographical scales could significantly expand our understanding of tropical forest structure. A comprehensive database of forest structure "fingerprints" could prove instrumental in detecting disturbances, monitoring ecosystem health, and aiding in biodiversity conservation.

CRediT authorship contribution statement

Nathan Borges Gonçalves: Writing – review & editing, Writing – original draft, Visualization, Validation, Methodology, Investigation, Formal analysis, Conceptualization. **Diogo Martins Rosa:** Writing – review & editing, Project administration, Methodology, Data curation, Conceptualization. **Dalton Freitas do Valle:** Writing – review & editing, Methodology, Investigation, Data curation, Conceptualization. **Marielle N. Smith:** Writing – review & editing, Writing – original draft, Data curation. **Ricardo Dalagnol:** Writing – review & editing, Writing – original draft. **Danilo Roberti Alves de Almeida:** Writing – review & editing, Methodology, Conceptualization. **Bruce W. Nelson:** Writing – review & editing, Writing – original draft, Methodology, Investigation, Funding acquisition, Formal analysis, Data curation, Conceptualization. **Scott C. Stark:** Writing – review & editing, Writing – original draft, Supervision, Methodology, Investigation, Funding acquisition, Formal analysis, Conceptualization.

Declaration of competing interest

None.

Data availability

Data will be made available on request.

Acknowledgements

We thank Brazil's National Institute for Amazon Research. The Brazilian Ministry of Science, Technology and Innovation (MCTI/FINEP contract 01.11.01248.00). NB Gonçalves, SC Stark and MN Smith were supported by NSF DEB awards no. 1950080 and 1754357. NB Gonçalves was also financed by Michigan State University Mericle Memorial Fund.

Appendix A. Supplementary data

Supplementary data to this article can be found online at https://doi.org/10.1016/j.ecoinf.2024.102628.

References

Aleixo, I., Norris, D., Hemerik, L., Barbosa, A., Prata, E., Costa, F., Poorter, L., 2019. Amazonian rainforest tree mortality driven by climate and functional traits. Nat. Clim. Chang. 9 (5), 384–388.
Almeida, D.R.A.D., Stark, S.C., Chazdon, R., Nelson, B.W., César, R.G., Meli, P., Brancalion, P.H.S., 2019. The effectiveness of lidar remote sensing for monitoring forest cover attributes and landscape restoration. For. Ecol. Manag. 438, 34–43.
Araujo, R.F., Nelson, B.W., Celes, C.H.S., Chambers, J.Q., 2017. Regional distribution of large blowdown patches across Amazonia in 2005 caused by a single convective squall line. Geophys. Res. Lett. 44 (15), 7793–7798.
Atkins, J.W., Bond-Lamberty, B., Fahey, R.T., Haber, L.T., Stuart-Haëntjens, E., Hardiman, B.S., Gough, C.M., 2020. Application of multidimensional structural characterization to detect and describe moderate forest disturbance. Ecosphere 11 (6), e03156.
Bank, D., Koenigstein, N., Giryes, R., 2023. Autoencoders. In: Machine Learning for Data Science Handbook: Data Mining and Knowledge Discovery Handbook, pp. 353–374.
Belgiu, M., Drăguţ, L., 2016. Random forest in remote sensing: a review of applications and future directions. ISPRS J. Photogramm. Remote Sens. 114, 24–31.
Carrascal, L.M., Galván, I., Gordo, O., 2009. Partial least squares regression as an alternative to current regression methods used in ecology. Oikos 118 (5), 681–690.
Castilho, C.V., Magnusson, W.E., de Araújo, R.N.O., Luizao, R.C., Luizao, F.J., Lima, A.P., Higuchi, N., 2006. Variation in aboveground tree live biomass in a central Amazonian Forest: effects of soil and topography. For. Ecol. Manag. 234 (1–3), 85–96.
Chauvel, A., Lucas, Y., Boulet, R., 1987. On the genesis of the soil mantle of the region of Manaus, Central Amazonia, Brazil. Experientia 43, 234–241.
Costa, F.R., Schietti, J., Stark, S.C., Smith, M.N., 2023. The other side of tropical forest drought: do shallow water table regions of Amazonia act as large-scale hydrological refugia from drought? New Phytol. 237 (3), 714–733.
Cutler, D.R., Edwards Jr., T.C., Beard, K.H., Cutler, A., Hess, K.T., Gibson, J., Lawler, J.J., 2007. Random forests for classification in ecology. Ecology 88 (11), 2783–2792.
Dalagnol, R., Wagner, F.H., Galvão, L.S., Streher, A.S., Phillips, O.L., Gloor, E., Aragão, L. E., 2021. Large-scale variations in the dynamics of Amazon forest canopy gaps from airborne lidar data and opportunities for tree mortality estimates. Sci. Rep. 11 (1), 1388.
Dalagnol, R., Wagner, F.H., Emilio, T., Streher, A.S., Galvão, L.S., Ometto, J.P., Aragao, L.E., 2022. Canopy palm cover across the Brazilian Amazon forests mapped with airborne LiDAR data and deep learning. Remote Sens. Ecol. Conserv. 8 (5), 601–614.
Deng, J., Dong, W., Socher, R., Li, L.J., Li, K., Fei-Fei, L., 2009, June. Imagenet: A large-scale hierarchical image database. In: In 2009 IEEE Conference on Computer Vision and Pattern Recognition. Ieee, pp. 248–255.
Detto, M., Muller-Landau, H.C., Mascaro, J., Asner, G.P., 2013. Hydrological networks and associated topographic variation as templates for the spatial organization of tropical forest vegetation. PLoS One 8 (10), e76296.
Ehbrecht, M., Seidel, D., Annighöfer, P., Kreft, H., Köhler, M., Zemp, D.C., Puettmann, K., Nilus, R., Babweteera, F., Willim, K., Stiers, M., 2021. Global patterns and climatic controls of forest structural complexity. Nat. Commun. 12 (1), 519.

EMBRAPA, 1997. Centro Nacional de Pesquisa de Solos. Manual de métodos de análise de solo. Embrapa solos, Rio de Janeiro, RJ, Brazil.
Esteban, E.J., Castilho, C.V., Melgaço, K.L., Costa, F.R., 2021. The other side of droughts: wet extremes and topography as buffers of negative drought effects in an Amazonian forest. New Phytol. 229 (4), 1995–2006.
Fahey, R.T., Atkins, J.W., Gough, C.M., Hardiman, B.S., Nave, L.E., Tallant, J.M., Curtis, P.S., 2019. Defining a spectrum of integrative trait-based vegetation canopy structural types. Ecol. Lett. 22 (12), 2049–2059.
Fasiolo, M., Nedellec, R., Goude, Y., Wood, S.N., 2020. Scalable visualization methods for modern generalized additive models. J. Comput. Graph. Stat. 29 (1), 78–86.
Gonçalves, N.B., Dalagnol, R., Wu, J., Pontes-Lopes, A., Stark, S.C., Nelson, B.W., 2023. Amazon forest spectral seasonality is consistent across sensor resolutions and driven by leaf demography. ISPRS J. Photogramm. Remote Sens. 196, 93–104.
Gorgens, E.B., Nunes, M.H., Jackson, T., Coomes, D., Keller, M., Reis, C.R., Valbuena, R., Rosette, J., de Almeida, D.R., Gimenez, B., Cantinho, R., 2021. Resource availability and disturbance shape maximum tree height across the Amazon. Glob. Chang. Biol. 27 (1), 177–189.
Gorgens, E.B., Keller, M., Jackson, T., Marra, D.M., Reis, C.R., de Almeida, D.R.A., Coomes, D., Ometto, J.P., 2023. Out of steady state: tracking canopy gap dynamics across Brazilian Amazon. Biotropica 55, 755–766.
Hardiman, B.S., Bohrer, G., Gough, C.M., Vogel, C.S., Curtis, P.S., 2011. The role of canopy structural complexity in wood net primary production of a maturing northern deciduous forest. Ecology 92 (9), 1818–1827.
He, K., Zhang, X., Ren, S., Sun, J., 2016. Deep residual learning for image recognition. In: Proceedings of the 2016 IEEE Conference on Computer Vision and Pattern Recognition, pp. 770–778.
Howard, J., Gugger, S., 2020. Fastai: a layered API for deep learning. Information 11 (2), 108.
Jucker, T., 2022. Deciphering the fingerprint of disturbance on the three-dimensional structure of the world's forests. New Phytol. 233 (2), 612–617.
Jucker, T., Bongalov, B., Burslem, D.F., Nilus, R., Dalponte, M., Lewis, S.L., et al., 2018. Topography shapes the structure, composition and function of tropical forest landscapes. Ecol. Lett. 21 (7), 989–1000.
Kingma, D.P., Welling, M., 2019. An introduction to variational autoencoders. Found. Trends® Mach. Learn. 12 (4), 307–392.
Klauberg, C., Vogel, J., Dalagnol, R., Ferreira, M.P., Hamamura, C., Broadbent, E., Silva, C.A., 2023. Post-hurricane damage severity classification at the individual tree level using terrestrial laser scanning and deep learning. Remote Sens. 15 (4), 1165.
Kuhn, M., 2008. Building predictive models in R using the caret package. J. Stat. Softw. 28, 1–26.
LaRue, E.A., Fahey, R.T., Alveshere, B.C., Atkins, J.W., Bhatt, P., Buma, B., Fei, S., 2023. A theoretical framework for the ecological role of three-dimensional structural diversity. Front. Ecol. Environ. 21 (1), 4–13.
Lee, H., Pham, P., Largman, Y., Ng, A., 2009. Unsupervised feature learning for audio classification using convolutional deep belief networks. Advances in neural information processing systems, p. 22.
Li, W., Guo, W.Y., Pasgaard, M., Niu, Z., Wang, L., Chen, F., Svenning, J.C., 2023. Human fingerprint on structural density of forests globally. Nat. Sustain. 1–12.
Liaw, A., Wiener, M., 2002. Classification and regression by randomForest. R News 2 (3), 18–22.
Lopes, A.P., Nelson, B.W., Wu, J., de Alencastro Graça, P.M.L., Tavares, J.V., Prohaska, N., Saleska, S.R., 2016. Leaf flush drives dry season green-up of the Central Amazon. Remote Sens. Environ. 182, 90–98.
Luizão, R.C.C., Luizão, F.J., Paiva, R.Q., Monteiro, T.F., Sousa, L.S., Kruijt, B., 2004. Variation of carbon and nitrogen cycling processes along a topographic gradient in a Central Amazonian forest. Glob. Chang. Biol. 10, 592–600.
McGinn, K., Kahl, S., Peery, M.Z., Klinck, H., Wood, C.M., 2023. Feature embeddings from the BirdNET algorithm provide insights into avian ecology. Eco. Inform. 74, 101995.
Murphy, B.A., May, J.A., Butterworth, B.J., Andresen, C.G., Desai, A.R., 2022. Unraveling forest complexity: resource use efficiency, disturbance, and the structure-function relationship. Journal of geophysical research. Biogeosciences 127 (6), e2021JG006748.
Nobre, A.D., Cuartas, L.A., Hodnett, M., Rennó, C.D., Rodrigues, G., Silveira, A., Saleska, M., 2011. Height above the nearest drainage – a hydrologically relevant new terrain model. J. Hydrol. 404, 13–29.
Parker, G.G., Russ, M.E., 2004. The canopy surface and stand development: assessing forest canopy structure and complexity with near-surface altimetry. For. Ecol. Manag. 189, 307–315.
Parker, G.G., Harding, D.J., Berger, M.L., 2004. A portable LIDAR system for rapid determination of Forest canopy structure. J. Appl. Ecol. 41, 755–767.
Pedregosa, et al., 2011. Scikit-learn: machine learning in Python. JMLR 12, 2825–2830.
Quesada, C.A., Phillips, O.L., Schwarz, M., Czimczik, C.I., Baker, T.R., Patiño, S., et al., 2012. Basin-wide variations in Amazon Forest structure and function are mediated by both soils and climate. Biogeosciences 9 (6), 2203–2246.
R Core Team, 2020. R: A Language and Environment for Statistical Computing. R Foundation for Statistical Computing. https://www.R-project.org/.
Reis, C.R., Jackson, T.D., Gorgens, E.B., Dalagnol, R., Jucker, T., Nunes, M.H., Ometto, J. P., Aragão, L.E.O.C., Rodriguez, L.C.E., Coomes, D.A., 2022. Forest disturbance and growth processes are reflected in the geographical distribution of large canopy gaps across the Brazilian Amazon. J. Ecol. 110 (12), 2971–2983. https://doi.org/10.1111/1365-2745.14003.
Rennó, C.D., Nobre, A.D., Cuartas, L.A., Soares, J.V., Hodnett, M.G., Tomasella, J., Waterloo, M.J., 2008. HAND, a new terrain descriptor using SRTM-DEM: mapping Terra-firme rainforest environments in Amazonia. Remote Sens. Environ. 112, 3469–3481.
Rödig, E., Cuntz, M., Rammig, A., Fischer, R., Taubert, F., Huth, A., 2018. The importance of forest structure for carbon fluxes of the Amazon rainforest. Environ. Res. Lett. 13 (5), 054013.
Rosa, D.M., Nelson, B.W., do Valle, D.F., de Almeida, J.S., de Almeida, D.R.A., Stark, S.C., Saleska, S.R., Lefsky, M., 2017. Forest structure gradient along a Central Amazon catena revealed by ground LiDAR.
Scheeres, J., de Jong, J., Brede, B., Brancalion, P.H., Broadbent, E.N., Zambrano, A.M.A., et al., 2023. Distinguishing forest types in restored tropical landscapes with UAV-borne LIDAR. Remote Sens. Environ. 290, 113533.
Schietti, J., Emilio, T., Rennó, C.D., Drucker, D.P., Costa, F.R., Nogueira, A., et al., 2014. Vertical distance from drainage drives floristic composition changes in an Amazonian rainforest. Plant Ecol. Diversity 7 (1–2), 241–253.
Simonetti, A., Araujo, R.F., Celes, C.H.S., da Silva e Silva, F.R., dos Santos, J., Higuchi, N., Magnabosco Marra, D., 2023. Canopy gaps and associated losses of biomass–combining UAV imagery and field data in a Central Amazon forest. Biogeosciences 20 (17), 3651–3666.
Smith, M.N., Stark, S.C., Taylor, T.C., Ferreira, M.L., de Oliveira, E., Restrepo-Coupe, N., Saleska, S.R., 2019. Seasonal and drought-related changes in leaf area profiles depend on height and light environment in an Amazon forest. New Phytol. 222 (3), 1284–1297.
Smith, M.N., Stark, S.C., Taylor, T.C., Schietti, J., de Almeida, D.R.A., Aragón, S., Nelson, B.W., 2023. Diverse anthropogenic disturbances shift Amazon forests along a structural spectrum. Front. Ecol. Environ. 21 (1), 24–32.
Sousa, T.R., Schietti, J., Ribeiro, I.O., Emílio, T., Fernández, R.H., Ter Steege, H., Castilho, C.V., Esquivel-Muelbert, A., Baker, T., Pontes-Lopes, A., Silva, C.V., 2022. Water table depth modulates productivity and biomass across Amazonian forests. Glob. Ecol. Biogeogr. 31 (8), 1571–1588.
Stark, S.C., Schietti, J., Wu, J., Brando, V.O.B., Parker, G.G., Smith, M.N., 2012. Amazon forest carbon dynamics predicted by profiles of canopy leaf area and light environment. Ecol. Lett. 15 (12), 1406–1414.
Suominen, L., Ruokolainen, K., Pitkänen, T., Tuomisto, H., 2015. Similar understorey structure in spite of edaphic and floristic dissimilarity in Amazonian forests. Acta Amazon. 45, 393–404.
Toledo, M., Poorter, L., Peña-Claros, M., Alarcón, A., Balcázar, J., Leaño, C., Bongers, F., 2011. Climate is a stronger driver of tree and forest growth rates than soil and disturbance. J. Ecol. 99 (1), 254–264.
Wickham, H., 2016. ggplot2: Elegant Graphics for Data Analysis. Springer-Verlag, New York. ISBN 978–3–319-24277-4. https://ggplot2.tidyverse.org.
Wood, S.N., 2011. Fast stable restricted maximum likelihood and marginal likelihood estimation of semiparametric generalized linear models. J. R. Stat. Soc. Ser. B Stat Methodol. 73 (1), 3–36.
Wu, J., Albert, L.P., Lopes, A.P., Restrepo-Coupe, N., Hayek, M., Wiedemann, K.T., Guan, K., Stark, S.C., Christoffersen, B., Prohaska, N., Tavares, J.V., 2016. Leaf development and demography explain photosynthetic seasonality in Amazon evergreen forests. Science 351 (6276), 972–976.
Zhao, Q., Adeli, E., Honnorat, N., Leng, T., Pohl, K.M., 2019. Variational autoencoder for regression: Application to brain aging analysis. In: Medical Image Computing and Computer Assisted Intervention–MICCAI 2019: 22nd International Conference, Shenzhen, China, October 13–17, 2019, Proceedings, Part II, Vol. 22. Springer International Publishing, pp. 823–831.
Ziegler, A., König, I.R., 2014. Mining data with random forests: current options for real-world applications. Wiley Interdiscip. Rev. Data Min. Knowledge Discov. 4 (1), 55–63.